Bangladesh J. Bot. **46**(3): 1079-1087, 2017 (September) Supplementary

METHOD FOR THREE DIMENSIONAL VISUALIZATION OF PLANT LESION APPEARANCE

XU JING[1], MIAO TENG[1,2,3*], YANG TAO[1], XU TONGYU[1], JI JIANWEI[1], JIN LI[1] AND LI QINGJI[1]

Shenyang Agricultural University, College of Information and Electrical Engineering, ShenYang, 110866, China

Keywords: Virtual plant, Three-dimensional plant visualization, Plant disease simulation, Appearance models

Abstract

Simulation of disease lesion on the surface of plant organ is a tough task due to the difficulty of the dynamic lesion appearance data acquisition. A method for three-dimensional visualization of plant disease appearance is presented only using lesion images. Given a single lesion image, the framework first extracts static appearance properties (e.g., lesion shape, diffuse reflectance, and texture), and deduces time-varying dynamic transition processes of these properties based on intrinsic decomposition. To simulate the spatial-varying appearance of disease on the plant organ surface, the user indicates to the framework the lesion distribution information(e.g., position, size, and direction) by simple interactions. A time-varying appearance model is also proposed for simulating the weathering appearance of the plant disease lesion. The experimental results demonstrate that the proposed method can realistically render appearances of various disease lesion types, and it has significant potential to be used as an effective visualization tool for decision making and education training in the field of agriculture.

Introduction

Three dimensional (3D) visualization is usually used as a support tool for decision making (Peng *et al*. 2010, Milien *et al*. 2012, Thiele *et al*. 2014, Kubicek *et al*. 2013, Barnert *et al*. 2014, Neethirajan *et al*. 2015, Han *et al*. 2016, Griffon *et al*. 2016, Urtė *et al*. 2016) and education/ training (Matsuda *et al*. 2005, Livingstone *et al*. 2008, Kotsilieris *et al*. 2013).Moreover, 3D modeling and visualization of plant appearance is a fundamental task in agricultural visualization. Plant disease is a common agricultural problem that can cause severe changes in plant organ appearance, such as discoloration, mildew, and corruption. By using state-of-the-appearance visualization technology, the measurement of real appearance materials can provide the most accurate data sets of the highest quality and simulate reliable and credible plant organ images (Wang *et al*. 2005, Habel *et al*. 2007). While complete plant disease material for appearance measuring is very difficult to obtain because disease is a kind of time-varying biological phenomenon. Consequently, measurement work is inefficient in practice on account of the difficult inoculation and cultivation process of plant diseases, lengthy measurement times, and complex acquisition setups (Weyrich *et al*. 2009). Miao proposed a visual simulation method of crop disease state based on image (Miao *et al*. 2016). Its strategy is to use existing disease image from Internet to generate plant disease 3D animation, and can solve the problem of the lack of related apparent data information of plant lesion. While this method has two defects: (i) it is very sensitive to the light shading in image since the algorithm extracts appearance information directly on the

*Author for correspondence: <caumiao@126.com>.1.College of Information and Electrical Engineering, Shenyang Agricultural University, Shen Yang 110866, China; 2. Beijing Key Lab of Digital Plant, Beijing 100097, China; 3.National Engineering Research Center for Information Technology in Agriculture, Beijing 100097.

original image, which may lead to a lesion appearance be mistaken for a variety of appearances. (ii) The method uses green component in lesion color appearance to infer the morphology and appearance transition of lesion. In this case, the method will not be able to simulate some diseases like powdery mildew, which has white or black color appearance.

A more robust method for simulating plant organ appearance in a disease state based on image is presented. Similar to the method of Miao *et al*. (2016), we also focus on modeling the spatially-varying and time-varying diffuse appearance of a disease lesion from a single plant lesion texture image captured from a nearly planar illuminated surface. While, given an input disease lesion image, our method can remove the shading from lesion image, and use graph method to infer the morphology and appearance transition of lesion. The present method can generate compelling 3-D plant simulation results ranging from a healthy status to a disease status.

Materials and Methods

A method for 3D visualization of the time-spatial-varying plant lesion appearance has been presented. The core of the present frame work is an image process pipeline that can infer the morphology and appearance transition information of a lesion from a single image by employing simple user interactions. Our method consists of 3 steps: (i) First, we use intrinsic image decomposing method to remove the shading in an input plant lesion image and obtain a reflectance image, (ii) we infer the morphology and appearance change of plant lesion from the reflectance image by user interaction and graph method and (iii) we render 3d lesion appearance using a spatial-varying and time-varying ward model. Present approach was implemented using C++ programming language, open GL and open CV library on a PC with a 3.40-GHz Intel Core i7-4770 processor and an NVIDIA GeForce GTX 660 graphics card.

In order to remove the shading information in an input image, authors assume that the surfaces of plant organs and disease lesion are Lambertian. In this case, alesion red-green-blue (RGB) image*I,* can be decomposed into an illumination layer *S,* and a reflectance layer *R*. Accordingly, for each pixel *p* and each color channel *c(cε(r,g,b)*, the intrinsic image decomposition process can be expressed as

$$I_c(p) = R_c(p)S_c(p) \tag{1}$$

Furthermore, an optimization framework has also been used (Shen 2013) to obtain reasonable decomposition results. The reflectance value of one pixel can be represented by the weighted summation of its neighborhood pixel values as:

$$R_c(p_i) = \sum_{P_j \in N(P_i)} \omega_{ij} R_c(p_j)$$
$$\omega_{ij} = e^{-[<I'_c(p_i), I'_c(p_j)>^2 / \sigma_T(p_i) + (Y(p_i) - Y(p_j))^2 / \sigma_Y(p_i)]} \tag{2}$$

Where ω_{ij} measures the similarity of the reflectance between pixel p_i and pixel p_j. $N(p_i)$ denotes a local neighborhood window around pixel p_i (e.g., 3×3, 5×5). $[I'_c(p_i), I'_c(p_j)]$ denotes the angle between vector). $I'_c(p_i)$ and $I'_c(p_j)$. Additionally, $I'_c(p_i)$ is a normalized RGB triplet of $I'_c(p_i)$. Moreover, $\sigma_T(p_i)$ represents the variance of the angle between pixel p_i and the pixels in a local window around p_i. Meanwhile, $Y(p)$ is the intensity of pixel p. In the present implementation, the latter value is obtained by $0.299\ I_r\ (p)+0.587 I_g(p)+0.114 I_b(p)$. In addition, $\sigma_Y(p_i)$ represents the intensity variance between pixel p_i and the pixels in a local window around p_i.

The energy function has been defined to obtain the intrinsic images:

$$\mathbf{E}(R,S) = \sum_{p_i \in \mathbf{P}} \left(R(p_i) - \sum_{p_j \in \mathbf{N}(i)} [\omega_{ij} R(p_j)] \right)^2 + \sum_{p_i \in \mathbf{P}} \left(\frac{I(p_i)}{S(p_i)} - R(p_i) \right)^2 \quad (3)$$

where, prepresents all pixels in image. Then, the above equation is optimized to obtain the intrinsic images, including reflectance image R and shading image S:

$$arg_{R,S}\, E(R,S)$$
$$\forall 0 \le R_c(P_i) \le 1 \quad (4)$$

In the present implementation, a gradient descent method is used to optimize the above energy function and obtain the optimal solutions.

The appearance transition of a plant lesion due to disease infection is a kind of weathering phenomenon. In this paper, a diffuse transfer path D has been used consisting of several diffuse vectors to represent a gradual transition in the diffuse appearance of a lesion from the least weathered- to the most weathered state. The user first selects the region of interest (ROI), R', from reflectance image, R. Thus, R' into N diffuse sets by ak - means method according to pixel RGB channels are classified. In the present implementation, $N = 20$. The centroid vector of each diffuse setis considered a key diffuse feature in the lesion growth process. All centroid vectors are then utilized to construct an initial neighborhood graph that connects each vertex to its k-nearest neighbors ($k = 8$ in this paper). Each centroid vector is avertex in the graph. This graph is pruned by deleting the connection edge between points separated by a distance of more than a given threshold, ϵ. In the present implementation, $\epsilon = 2.0d$, where d is the average L_2 distance between connected points of the initial graph.

From the structure of the resulting neighborhood graph, our method infers D through user interactions. The user specifies the most and least weathering pixel, respectively, on ROI R'. The corresponding centroid vector (graph vertex), V_1 (weather edvertex), and V_2 (normal vertex) are selected from all 20 centroid vectors by determining the categories to which the two pixels belong. Dijkstra's algorithm (Dijkstra 1959) is utilized to compute the shortest path from V_1 to V_2 in the graph. This path is diffuse transfer path D. Path D includes a set of reflectance vectors describing the time-varying diffuse appearance, while the path vertex order represents the sequence of key diffuse features in the infection process. In this paper, path D is not directly employed to simulate the weathering process because the difference of adjacent vertices in D may make the transient process discontinuous and not visually smooth. Therefore, we generate more diffuse vectors between adjacent vertices. This expands the original path into a more compact diffuse set. In our implementation, linear interpolation is used to compute ten new diffuse vectors between two adjacent vertices. Then, the final diffuse transfer path D contains $(N - 1) \times 10 + N$ diffuse vectors. Finally, path D is saved as a 1D texture image for 3D lesion appearance synthesis.

Using path D, a weathering degree is computed $w(p)$ ($0.0 <= w <= 1.0$) for each lesion point p in image R indicates the degree of disease infection. The lesion pixels have been extracted first from reflectance image R by the Grab Cut (Rother *et al.* 2004) method. From that point, $w(p)$ for lesion point p with RGB vector $c(p)$ in image R is defined by

$$w(p) = \frac{\varnothing(G(c(p))) - 1}{(N - 1 * 10 + N} \quad (5)$$

where G(*) is the nearest diffuse vector of $c(p)$ in D. In addition, $\varnothing(\bullet)$ is the index number of G(•) in D. The denominator of the above equation is the total element number of the diffuse transfer path.

By computing the weathering degree values for all lesion pixels in image *R*, a weathering degree map was obtained (Fig. 2d). The map displays spatial variations in weathering degrees over the lesion.

A lesion distribution map has therefore been created for specifying the locations of all lesions on the organ surface. The lesion distribution map is a gray image, whose pixel intensity indicates the weathering degree of a point on the surface of plant organ. This was used to synthesize a detailed spatial-varying lesion appearance on the 3D model. It is difficult to determine accurately the appearance from the existing lesion images obtained from the Internet. This is because most of these lesion images illustrate lesions for which the location information is missing, and some images have image distortion due to the camera view, which makes the location information inaccurate. In the present implementation, this map was created by a manual specification. A simple interface called Lesion Distribution Map software (Fig. 3b) is used for adjusting parameters, such as lesion location, size, rotation angle, and weathering degree increment (or reduction), using a weathering degree map as input and the organ texture as a location reference.

The present method employs diffuse transfer paths and a lesion distribution map to synthesize the detailed lesion appearance onto a 3D plant organ model according to a given user-defined and time-variant global weathering parameter W ($W \geq 0$). The parameter W indicates the disease degree of the plant organ. A weathering degree parameter $w'(p)$ ($0 \leq w'(p) \leq 1$) is also defined for any point p on the 3D model to indicate the degree of disease infection on point p. A larger value represents a more serious infection situation. Weathering degree $w'(p)$ is calculated by

$$w'(p) = W - w(p') \qquad (6)$$

where, p' is the corresponding pixel in the lesion distribution map of point p, and $w(p')$ is the pixel value of p ($0 \leq w'(p') \leq 1$). From the above formula, it is evident that parameter W has a general effect on all points on the model, which thereby produces a time-variant lesion appearance effect. Parameter $w(p')$has different effects on different points, thereby conferring a spatial-variant appearance. With the increase of W, a larger $w(p')$makes the lesion appeared earlier on point p.

In the present method, a ward model is used for modeling the BRDF(Bidirectional Reflectance Distribution Function) of the plant organ and lesion. It specifies that surface point p reflects light from direction $(\Theta_i, \varnothing_i)$ to direction$(\Theta_r, \varnothing_r)$ with the following distribution of f_r:

$$f_r(\theta_i, \varnothing_i; \theta_r, \varnothing_r; p) = f_r^d(p) + f_r^s(\theta_i, \varnothing_i; \theta_r, \varnothing_r; p) = \frac{\rho_d(p)}{\pi} + \rho_s \frac{e^{-\left(\left[\tan\delta\right]\right]^2 / \beta^2}}{4\pi\beta^2\sqrt{\cos\theta_i \cos\theta_r}} \qquad (7)$$

In this equation, $f_r^d(p)$ and $f_r^s(\theta_i, \varnothing_i; \theta_r, \varnothing_r; p)$ are the diffuse term and specular term respectively. In addition, δ is the angle between the normal of p and the half vector between the incident and reflected directions. Meanwhile, ps, and β are the specular intensity component and specular roughness, respectively, and they are respectively set to 0.2 and 0.3 in the present implementation. Furthermore, $p$dcan be described by albedo texture for plant organs. Because the diffuse appearance of the lesion is time-varying and spatial-varying, we define $f_r^d(p)$ for the lesion by

$$f_r^d(p) = \frac{\rho_d(w'(p))}{\pi} \qquad (8)$$

Here, pd becomes a function of weathering degree $w'(p)$ and can be indexed from the diffuse transfer path with $w'(p)$ as the texture coordinate.

Some diseases, such as powdery mildew, for many gaps. Present authors simulate this apparent phenomenon by disturbing the BRDF f_r value (calculated by equation (7)) of every lesion

point. We use a perlin noise texture to assign a different random value for every lesion point and a same threshold value z for all the lesion points. If the random value at any lesion point is larger than z, the BRDF f_r value of this point is set 0.0, otherwise, the f_r value is calculated by equation (7).

Results and Discussion

The present method was tested with southern corn leaf blight lesion on maize and powdery mildew lesion on grape. Fig. 1 shows the results of our intrinsic lesion image decomposition approach. A Southern corn leaf blight lesion image (Fig. 1a) is decomposed into a reflectance image (Fig. 1b) and a shading image (Fig. 1c). The shading image contains the shadows and shading caused by illumination which makes some organ surface points with similar reflectance show a very different color appearance. Because the effect of illumination is removed in reflectance image, the color appearance in it is more refined and smooth than the original lesion image. In our method, we just use the appearance information in reflectance image, so we can get more accurate simulation results than traditional methods (Miao *et al.* 2016).

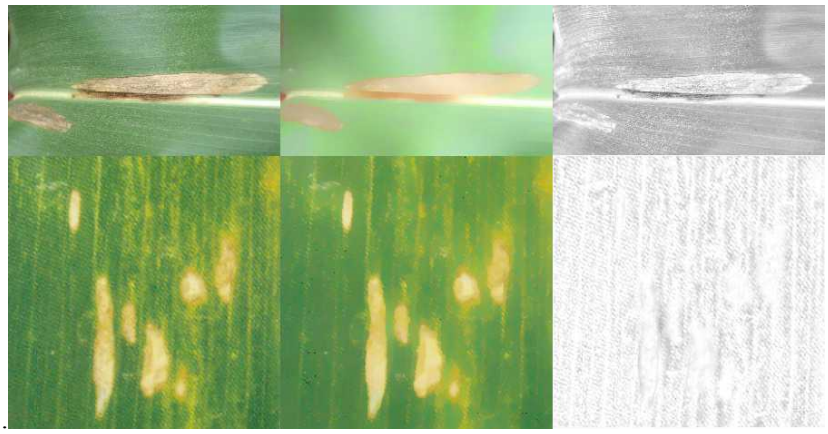

(a) (b) (c)

Fig.1. Results of intrinsic image decomposition. (a) Southern corn leaf blight lesion image, (b) reflectance image and (c) shading image.

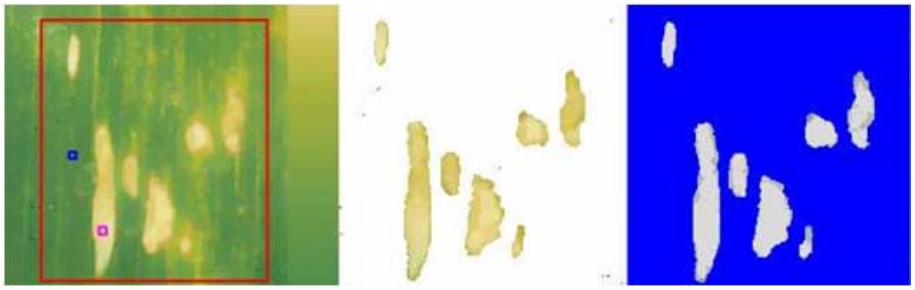

(a) (b) (c) (d)

Fig. 2. Inferred lesion morphology and appearance changes. (a) user specifies ROI (red rectangle), the most weather pixel (pink rectangle), and the normal pixel (blue rectangle), (b) diffuse transfer path. This path is saved as a 1D texture in our implementation. Here, a 2D texture image is shown to enhance the description, (c) lesion pixels extracted from the reflectance image and (d) weathering degree map. Blue pixels represent non-lesion pixels.

Fig. 2 shows the results of our approach for time-varying dynamic appearance inference. The diffuse transfer path (Fig. 2b) is continuous and natural, and weathering degree map (Fig. 2c) is smooth which shows that the starting point and end point of appearance transition obtained by artificial interaction is an accurate prior knowledge for the dynamic appearance inference. The graph method is also an effective scheme for constructing apparent dynamic processes.

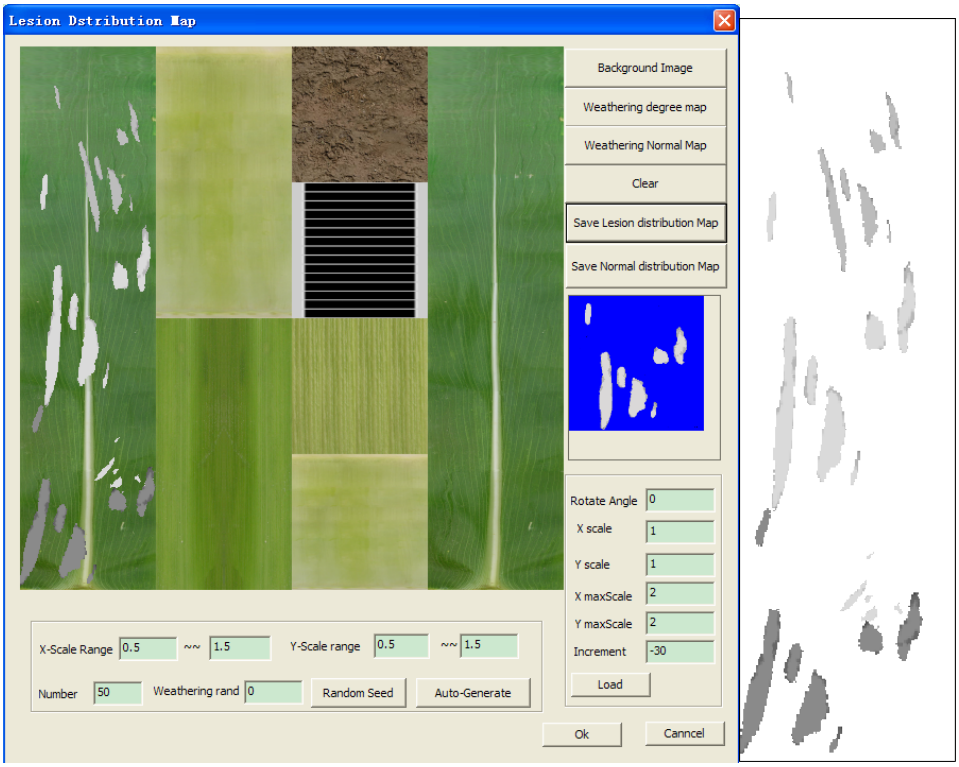

(a) (b)

Fig. 3. Lesion distribution map created by the Lesion Distribution Map software with user interactions. (a) Lesion Distribution Map software for specifying the lesion distribution, location, rotation angle, and weathering degree increment. The user implements the operation to reference the plant organ texture, which helps the user recognize the lesion location and (b) lesion distribution map generated by an operation similar to(a).

Fig. 3 shows the Lesion Dstribution Map software we developed for generating spatial-varying appearance information. This software gives users a lot of flexibility to introduce their prior knowledge and experience in the lesion spatial distribution.

Fig. 4 shows the simulation results of the time-spatial varying appearance of a *Helminthosporium maydi*s (Southern corn leaf blight) lesion on maize. This toxin leads to maize leaf chloros is and forms some oval lesions. Global weathering degrees W were set to 0.0, 0.2, 0.6 and 1.0, respectively from (a) to (d). The images of Figs 2b and 3b were used as the diffuse transfer path and lesion distribution map, respectively. Our visualization result is realistic and shows well the appearance information in the lesion image. This demonstrates the ability of our method in dynamic lesion appearance visualization from only static appearance properties in a single image.

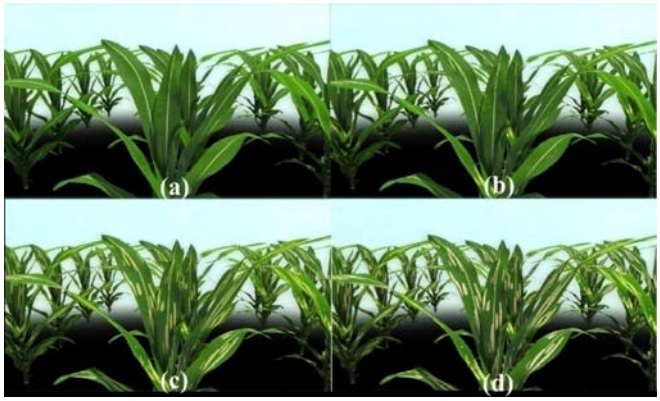

Fig. 4. Simulation of the appearance of a *Helminthosporium maydis* lesion of maize. (a) appearance with global weathering degree *W* equal to 0. The lesions do not appear on maize organs. (b) appearance with *W* equal to 0.2. Some lesions begin to appear in some leaf areas. (c) appearance with *W* equal to 0.6. At this stage, the lesion appear soval and yellow. (d) appearance with *W* equal to 1.0. The hue of the lesion changes to white. In the present framework, this stage represents the appearance of a lesion as the final state.

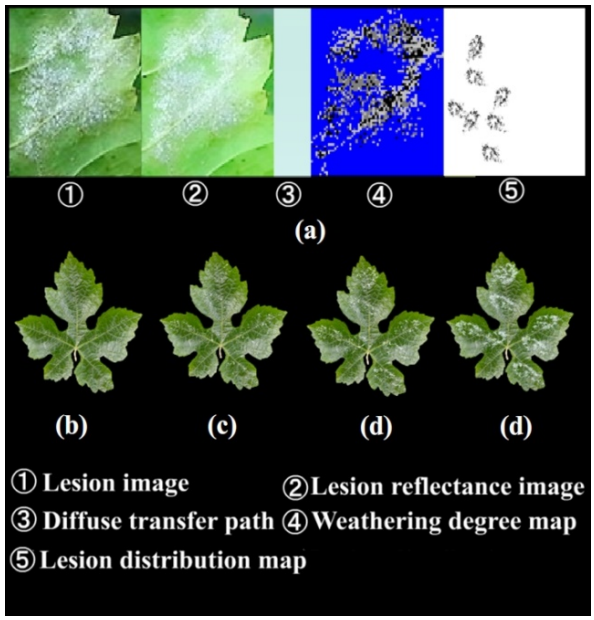

Fig. 5. Simulation of the appearance of powdery mildew on agrape leaf. (a) texture images used for 3D simulation, (b) appearance with global weathering degree *W* equal to 0, (c), appearance with *W* equal to 0.2. (d) appearance with *W* equal to 0.6, (e) appearance with *W* equals equal to1.0.

Fig. 5 shows the appearance of powdery mildew on a grape leaf. Powdery mildew forms a granular-layer structure on the leaf surface. Global weathering degrees *W* is set to 0.0, 0.2, 0.6, and 1.0, respectively, from (b) to (e). This indicates how compelling 3-D plant simulation could simulate diseases in black and white appearance which could not be realized by traditional simulation methods (Miao *et al.* 2016).

Table 1 provides detailed performance of our framework. The most time-consuming step of our method is intrinsic image decomposing. As the resolution of the input lesion image increases, the running time shows nonlinear growth. This is because our optimization framework for intrinsic decomposing needs to integrate the neighborhood information of each pixel for iterative computation, and a high resolution image will increase the number of neighboring pixels and the number of iterations. While the lesion images with 1024 × 1024 resolution have enough information for appearance properties extracting. Ten seconds or so is tolerable for the entire algorithm flow. The dynamic appearance inference step and 3D appearance visualization step all have real-time processing speed. They guarantee that user can get the WYSIWYG processing results in these two steps. In general, our approach has a very fast data analysis and visualization speed, which is a very important feature for a visual tool.

Table 1. Performance of our method.

Approach name	Image resolution	3d modeland texture size (Mb)	Running time (second)
Intrinsic image decomposing	512×512	None	3.300
Intrinsic image decomposing	1024×1024	None	10.7
Dynamic appearance inference	512×512	None	0.300
Dynamic appearance inference	1024×1024	None	0.520
3D appearance visualization	None	190.8	0.017
3D appearance visualization	None	100.6	0.009

The experimental results showed that the present framework works well for a variety of disease lesion types and has significant potential to become an effective visualization tool for decision making and education and training. Currently, the method mainly uses user interactions for specifying lesion distributions on plant organ surfaces. In future research, developing intelligent methods to automatically estimate more accurate lesion distribution information will be focused.

Acknowledgements

The research is supported by the National Natural Science Foundation of China (Grant No. 31501217), Beijing Municipal Natural Science Foundation (Grant No.4162028), National Natural Science Foundation of China (61673281), National Natural Science Foundation of China (31601218), Science research project of Liaoning Provincial Department of Education (L2015484) and Science research project of Liaoning Provincial Department of Education (L2014265).

References

Barnert T, Piesik E and Śliwiński M 2014. Real-time simulator of agricultural biogas plant. Comput. Electron. Agr. **108**: 1-11

Dial RB 1969. Algorithm 360: shortest-path forest with topological ordering. ACMCOMMUN **12**(11): 632-633.

Dijkstra EW 1959. A Note on Two Problems in Connection with Graphs [J]. NUMER MATH **1**(1): 269-271.

Griffon S and Coligny FD 2014. Amapstudio: An editing and simulation software suite for plants architecture modeling. Ecol. Model. **290**: 3-10.

Habel R, Kustering A and Wimmer M 2007. Physically based real-time translucency for leaves. Proceeding of the 18th Eurographics conference on rendering techniques. Aire-la-Ville: Eurographics Association Press. pp. 253-263.

Han YY, Wu BG, Wang KY, Guo EY, Dong C and Wang ZB 2016. Individual-tree form growth models of visualization simulation for managed larixprincipis-rupprechtii, plantation. Comput. Electron. Agr. **123**(C): 341-350.

Kotsilieris T and Dimopoulou N 2013. The evolution of e-learning in the context of 3D virtual worlds.[J]. EJEL **11**:147-167

Kubicek P, Kozel J, Stampach R and Lukas V 2013. Prototyping the visualization of geographic and sensor data for agriculture. Comput. Electron. Agr. **97**(97): 83-91.

Livingstone D, Kemp J and Edgar E 2008. From multi-user virtual environment to 3D virtual learning environment [J]. ALT-J **16**(3):139-150

Matsuda H and ShindoY 2005. Self e-learning system using interactive real-time 3D computer graphics animations. J. Inst. Image Inf. Telev. Eng. **59**(11):1659-1668

Miao T, Guo XY and Wen WL *et al.* 2016. Three dimensional visual simulation method of crop disease state based on image. Trans. Chin. Soc. Agric. Eng. **32**(7):181-186.

Milien M, Renault-Spilmont AS, Cookson SJ, Sarrazin A and Verdeil JL 2012. Visualization of the 3d structure of the graft union of grapevine using x-ray tomography. Sci. Hort. **144**(3):130-140

Neethirajan S 2015. Real-time 3d visualization and quantitative analysis of internal structure of wheat kernels. J. Cereal Sci. **63**: 81-87

RotherC, KolmogorovV. and Blake A 2004. GrabCut: Interactive foreground extraction using iterated graph cuts. ACM SIGGRAPH. **23**: 309-314

Peng H and Long F 2010. V3d enables real-time 3d visualization and quantitative analysis of large-scale biological image data sets. Nat. Biotech. **28**(4): 348-53.

Shen J, Yang X and Li X *et al.* 2013. Intrinsic image decomposition using optimization and user scribbles. IEEE T Cyber. **43**(2): 425-436.

Thiele H, Heldmann S, Trede D, Strehlow J, Wirtz S and Dreher W *et al.* 2014. 2d and 3d maldi-imaging: conceptual strategies for visualization and data mining. Biochim. Biophysica Acta **1844**(1 PtA): 117-137.

Wang LF, Wang WL, Dorsey J, Yang K and Guo BN 2005. Real-time rendering of plant leaves. Acm. T. Graphic. **24**(3): 712-719.

Weyrich T, Lawrence J, Lensch HPA *et al.* 2009. Principles of appearance acquisition and representation. Found. Trends ® Comp. Graph.Vision **4**(2): 75-191.

Urtė R and Rimantas K 2016. Determining the shape of agricultural materials using spherical harmonics. Comput. Electron. Agr. **128**: 160-171.

(Manuscript received on 14 April, 2017; revised on 21 August, 2017)